JACS
JOURNAL OF THE AMERICAN CHEMICAL SOCIETY
Article
pubs.acs.org/JACS

Structural Isomers of Ti_2O_4 and Zr_2O_4 Anions Identified by Slow Photoelectron Velocity-Map Imaging Spectroscopy

Jongjin B. Kim, Marissa L. Weichman, and Daniel M. Neumark*

Department of Chemistry, University of California, and Chemical Sciences Division, Lawrence Berkeley National Laboratory, Berkeley, California 94720, United States

Supporting Information

ABSTRACT: High-resolution anion photoelectron spectra are reported for the group 4 metal dioxide clusters $Ti_2O_4^-$ and $Zr_2O_4^-$. Slow photoelectron velocity-map imaging (SEVI) spectroscopy of cryogenically cooled, mass-selected anions yields photoelectron spectra with submillielectronvolt resolution, revealing extensive and well-resolved vibrational progressions. By comparison of the spectra with Franck−Condon simulations, we have identified the C_{2v} and C_{3v} isomers as the ground states of $Ti_2O_4^-$ and $Zr_2O_4^-$ anions, respectively. Minor contributions from the C_{2h} isomer of $Ti_2O_4^-$ and the C_{2v} isomer of $Zr_2O_4^-$ are also seen. The SEVI spectra yield upper bounds for the adiabatic detachment energies, as well as vibrational frequencies for various modes of the neutral Ti_2O_4 and Zr_2O_4 species.

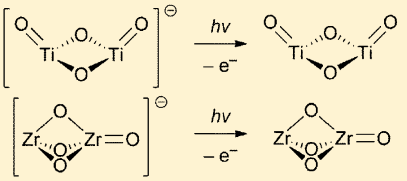

1. INTRODUCTION

Titanium oxide and zirconium oxide are technologically important materials, with wide applications in pigments, refractory ceramics, catalysis, and photochemistry.[1−5] Although the surface chemistry of the bulk oxide materials has been extensively studied,[1,6,7] a considerable effort has also been made in understanding the structure and reactivity of small metal oxide clusters, including $(MO_2)_n$ (M = Ti, Zr) clusters. Point defects in bulk materials can be important catalytically active sites, and isolated gas-phase clusters can be used as structural and reactive analogues that are more tractable for detailed study.[8−10] Transition metal oxide clusters exhibit different structural motifs than those found in the bulk material, and attempts have been made to predict and observe the relevant sizes and the consequences of these motifs for their reactive chemistry.[11−14] Spectroscopic characterization of polymetal oxide clusters has proved challenging, although some of these species have been investigated by matrix isolation infrared spectroscopy,[15] photoelectron (PE) spectroscopy,[13,14,16] and infrared photodissociation (IRPD) spectroscopy.[12] Compared to the other methods, photoelectron spectroscopy is perhaps the most general but its resolution is typically lower; in particular, vibrational structure is often not resolved for metal oxide clusters. We report the first high-resolution photoelectron spectra of anionic polynuclear transition metal oxides by combining cryogenic ion cooling with slow electron velocity-map imaging, yielding extensive and well-resolved vibrational progressions. By comparing the experimental and calculated spectra, we identify the most stable gas-phase $M_2O_4^-$ isomers as well as the next most stable isomers.

Bulk titania and zirconia have large bandgaps due to fully oxidized metal centers and are both formally d^0 systems, but they adopt different structures.[17,18] While ZrO_2 has a single monoclinic crystal form at ambient conditions, TiO_2 is found naturally in anatase, rutile, and brookite forms. Metal oxide clusters can have dramatically different structures than those found in the bulk material, and the transition between the two regimes is not well-understood.[11,19] Moreover, titanium and zirconium oxide clusters show strong size-dependent reactivity with various molecules of catalytic interest, suggesting that an understanding of cluster properties may lead to a better understanding of what controls their reactivity.[20−23] It is therefore of considerable interest to track the evolution of metal oxide structures with cluster size.

Several spectroscopic methods have been applied to titanium and zirconium oxide clusters. Photoionization mass spectrometry showed that, in the presence of oxygen, the most stable neutral clusters have M_nO_{2n} and M_nO_{2n+1} composition.[24,25] IR resonance-enhanced multiphoton ionization spectroscopy yielded IR spectra of neutral titanium and zirconium oxide clusters. The observed cluster compositions were generally deficient in oxygen, likely due to less-oxidized clusters possessing a lower ionization potential, and only broad vibrational features were resolved.[26,27] Anion PE spectra[28,29] have been obtained for titanium oxide anion clusters with an emphasis on determining the electron affinity and band gap of $(TiO_2)_n$ as a function of cluster size for n = 1−10; this latter property is one of the key characteristics determining the photochemistry of bulk TiO_2.

More detailed spectroscopy has been performed on specific $(MO_2)_n$ clusters. The vibronic structure and geometries of triatomic TiO_2 and ZrO_2 have been characterized by a variety of techniques.[30−35] However, less is known about the next smallest $(MO_2)_2$ clusters. The M_2O_4 clusters have been isolated in an inert gas matrix and well-resolved IR vibrational spectra have been obtained of those species.[36] Anion PE spectra have been reported for $Ti_2O_4^-$, but the electron kinetic energy

Received: March 17, 2014
Published: May 5, 2014

   dx.doi.org/10.1021/ja502713v | J. Am. Chem. Soc. 2014, 136, 7159−7168

resolution of 30 meV was insufficient to resolve any vibrational structure.[28,29]

These experiments require comparison with theory for their interpretation. Titanium oxide cluster geometries have been determined by Hartree−Fock theory,[37] various density functional methods,[38−41] simulated annealing methods refined by density functional theory,[42,43] an evolutionary algorithm,[44] and coupled-cluster theory.[45] Similarly, structures of zirconium oxide clusters have been calculated by density functional theory (DFT),[26,46] an evolutionary algorithm to find the global minimum,[47] and coupled-cluster theory.[48] Calculations agree with experiments on the structures and energies of the MO_2 triatomic species, but there is more uncertainty on the $n = 2$ clusters. Electronic structure calculations indicate that the lowest energy structures for the neutral and anionic clusters are C_{2v}, C_{2h}, or C_{3v} isomers (Figure 1),[37,38,40,45,47,48] with either two

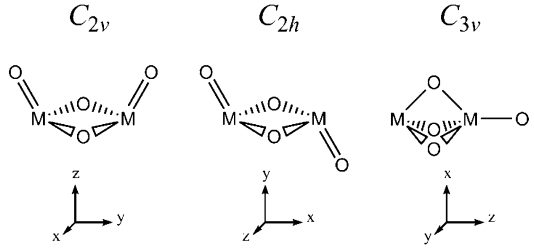

Figure 1. Schematic structures for the three M_2O_4 (M = Ti, Zr) structural isomers considered in this work. The axis convention chosen is also shown to highlight the axis of highest symmetry and the b_1 vs b_2 convention chosen for the C_{2v} isomer.

or three oxygen atoms bridging the metal atoms. Other structures have been considered, but they are consistently found to be higher in energy and are not considered in this work.[40,45,47] While calculations have agreed upon the C_{2h} isomer as the stable neutral form of Ti_2O_4, in agreement with the matrix isolation IR study,[36] there is more disagreement about the structure of the anions. Different methods have variously identified all three isomers as the most stable forms of $Ti_2O_4^-$ and $Zr_2O_4^-$.[38,40,45,48] Zhai and Wang[29] assigned the ground state of $Ti_2O_4^-$ to the C_{3v} isomer by comparing experimental and calculated vertical detachment energies.

The highest level calculations to date, at a coupled-cluster level and complete basis set extrapolation [CCSD(T)/CBS], were carried out by Li and Dixon.[45,48] They found the C_{2v} and C_{3v} isomers of $Ti_2O_4^-$ and $Zr_2O_4^-$, respectively, to be the most stable, but the other isomers are very close in energy. Moreover, their calculated $Ti_2O_4^-$ detachment energies for all isomers were compatible with the experimental PE results. The authors noted that, to make a definitive assignment of anion isomerism with PE spectroscopy, vibrational resolution and a comparison with Franck−Condon (FC) simulations are necessary. These calculations thus imply that probing the $M_2O_4^-$ species with a high-resolution anion PE technique could definitively resolve the question of which isomers are present.

In this work, we report slow electron velocity-map imaging (SEVI) spectra of cryogenically cooled $Ti_2O_4^-$ and $Zr_2O_4^-$. This combination of techniques results in PE spectra with submillielectronvolt resolution, yielding well-resolved progressions in low-frequency vibrational modes for both species. By comparing the experimental results with Franck−Condon simulations and calculated vibrational frequencies, we reassign the dominant feature in the $Ti_2O_4^-$ PE spectra to the C_{2v} isomer and identify a weak contribution from the C_{2h} isomer. The lowest-energy isomer of $Zr_2O_4^-$ is the C_{3v} isomer, but a small amount of the C_{2v} isomer is present. Vibrational frequencies of various modes are also assigned for the neutral M_2O_4 species.

2. EXPERIMENTAL SECTION

All experimental spectra were obtained with our high-resolution SEVI anion photoelectron spectrometer, the details of which have been described previously.[49−51] Anion metal oxide species are created in a laser ablation source, stored and cooled in a cryogenic ion trap, extracted into a time-of-flight mass spectrometer, and photodetached with a tunable laser. SEVI uses comparatively low extraction voltages on a velocity-map imaging (VMI) electron spectrometer,[52] allowing for high-resolution photoelectron spectra at low electron kinetic energies.

Titanium and zirconium oxide dimer anions were produced by laser ablation of a titanium or zirconium solid sample quenched by a pulse of helium gas. There were sufficient residual oxides in the metal and contaminant oxygen in the gas line for production of metal oxide ions. The ions were stored in an octopole ion trap held at 5 K and cooled by cryogenic buffer gas for 40 ms. A 20:80 mix of H_2/He was used to cool the $Zr_2O_4^-$ ions, conditions which have cooled ions down to 10 K.[51] We have previously found that including H_2 in the buffer gas enhances vibrational cooling of anions.[53] However, $Ti_2O_4^-$ reacts with H_2 to form a $Ti_2O_4H_2^-$ product, so the $Ti_2O_4^-$ ions were cooled with only helium as a buffer gas, possibly resulting in less efficient cooling.

After storage and cooling, the ions were extracted into a time-of-flight mass spectrometer and focused to the interaction region of a VMI spectrometer. The ion packets of the most abundant isotopologues, $^{48}Ti_2{}^{16}O_4^-$ and $^{90}Zr_2{}^{16}O_4^-$, were then photodetached with the output of a Nd:YAG-pumped tunable dye laser. The VMI electrostatic lens focused the photoelectrons to an imaging detector. The resulting 2D projection was used to reconstruct the 3D radial and angular velocity distribution by the maximum-entropy method MEVELER developed recently by Dick.[54]

The radial distribution gives the electron velocity and hence the electron kinetic energy (eKE) distribution. The best resolution of a VMI spectrometer is obtained at lowest kinetic energy; SEVI uses low extraction potentials to expand the image of the low-eKE, high-resolution components of a given photoelectron image, yielding spectra with submillielectronvolt resolution. To obtain a full set of high-resolution spectra, the laser wavelength was tuned in energy so that high-resolution spectra could be obtained for each region of interest. As intensities near threshold may depend on threshold partial-wave contributions,[55] the spectra were then scaled in intensity to the appropriate low-resolution overview spectrum and then combined. Each spectrum is plotted as a function of electron binding energy (eBE), given by eBE = $h\nu$ − eKE, where $h\nu$ is the photon energy used in that particular spectrum.

The photoelectron image also yields the photoelectron angular distribution (PAD). For photodetachment with linearly polarized light as in this experiment, the PAD is given by

$$\frac{d\sigma}{d\Omega} = \frac{\sigma_{tot}}{4\pi}\left[1 + \beta\left(\frac{3}{2}\cos^2\theta - \frac{1}{2}\right)\right] \quad (0)$$

where θ is the angle relative to the axis of polarization. The anisotropy parameter β varies from −1 to 2, giving the limits of a PAD perpendicular and parallel to the polarization axis.[56,57] As the value of β for a given transition varies with eKE, quantitative values are not reported here; the PAD is used mainly as a qualitative guide to distinguish between different electronic transitions.

3. THEORETICAL METHODS

Li and Dixon[45,48] calculated the energetics of the M_2O_4 anionic and neutral isomers at a benchmark CCSD(T)/CBS level. To compare their results with the experimental anion PE spectra of $Ti_2O_4^-$, they generated FC spectra for photodetachment from all three isomers at a

dx.doi.org/10.1021/ja502713v | J. Am. Chem. Soc. 2014, 136, 7159−7168

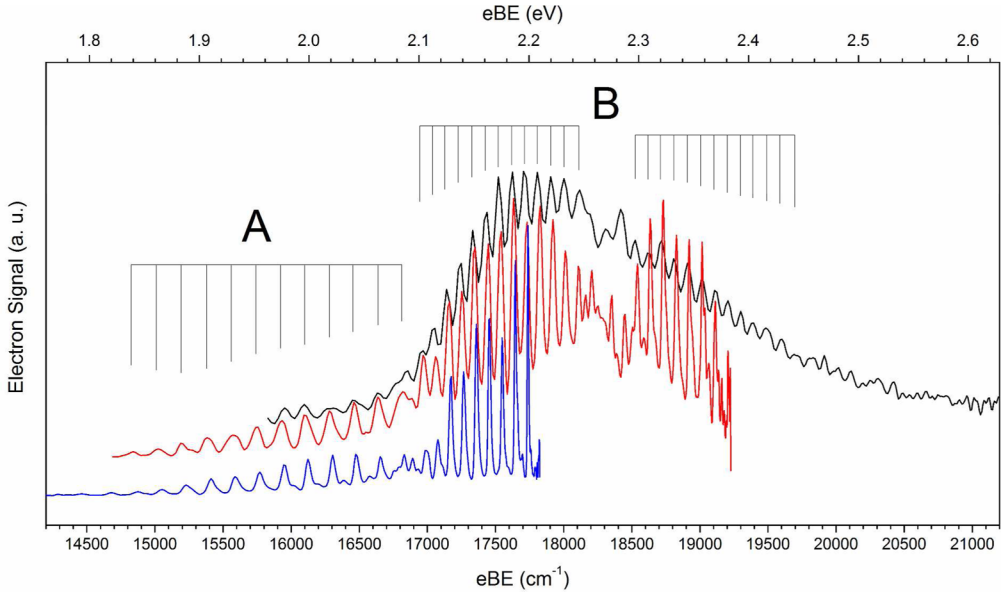

Figure 2. Overview spectra of Ti_2O_4, taken at three different photon energies of (blue) 17 824, (red) 19 226, and (black) 21 712 cm^{-1}. Spectra are offset vertically for clarity. The displayed combs emphasize the extended peak progressions in bands A and B.

less costly BP86/aug-cc-pVDZ-PP level. In order to account for typical experimental conditions in PE spectroscopy, they presented FC spectra with an ion vibrational temperature of 300 K and an instrumental resolution full width at half-maximum (fwhm) of 50 meV. Under these conditions, individual vibronic transitions are not resolved and only overall band profiles are distinguished. Although there were no experimental $Zr_2O_4^-$ spectra for comparison, they simulated FC spectra at the same level. In anticipation of higher-resolution techniques, they also simulated spectra with 1 meV resolution but still at a vibrational temperature of 300 K. SEVI with ion trapping and cooling, however, allows for submillielectronvolt resolution and vibrationally cold ions. Hence, for comparison with our experiments, we performed an independent set of electronic structure calculations and FC simulations assuming no anion vibrational excitation.

The work by Li and Dixon[45,48] also found that the BP86 density functional gave qualitatively similar geometries and energies compared to CCSD(T). Consequently, geometries and harmonic vibrational frequencies were determined with the BP86 functional. As with our previous study of group 4 triatomic metal dioxides,[35] the LANL2TZ basis set and the Hay-Wadt effective core potential were used for metal atoms,[58,59] while the 6-311+G* basis set was used for oxygen atoms. Electronic structure calculations, geometry optimizations, and vibrational analyses were all performed with Q-Chem 4.0.[60]

Franck−Condon simulations for the photodetachment spectra were made with the ezSpectrum program[61] in the harmonic approximation but with Duschinsky mixing of all modes. The experimental spectra have been obtained at differing resolution depending on the chosen photon energies. Therefore, the simulated spectra have been convolved with Gaussian distributions of different widths (15, 60, and 100 cm^{-1} fwhm) to facilitate comparison with experimental spectra.

4. RESULTS

4.1. Experiment. Photoelectron spectra of $Ti_2O_4^-$ and $Zr_2O_4^-$ are shown in Figures 2−5. Overview spectra of $Ti_2O_4^-$ are displayed in Figure 2, while higher-resolution spectra are shown in Figures 3 and 4, highlighting structure at eBEs between 14 000 and 17 000 cm^{-1} and between 16 500 and 17 800 cm^{-1}, respectively. The overview and high-resolution spectra of $Zr_2O_4^-$ are shown in Figure 5.

Owing to the dependence of energy resolution on eKE in the SEVI electron spectrometer, overview spectra for $Ti_2O_4^-$ are displayed at three different energies to highlight structure in different energy regions, from 14 500 to 21 000 cm^{-1}. There is a weak but extended progression of peaks beginning from ∼14 000 to 17 000 cm^{-1} (band A) that is then subsumed by a stronger spectral feature (band B). The high-resolution spectra encompassing band A (Figure 3) exhibit a main progression

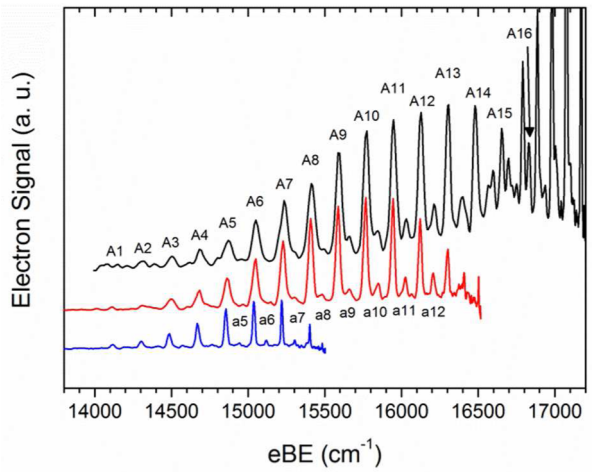

Figure 3. Representative SEVI spectra of C_{2h} Ti_2O_4 (band A), taken at three different photon energies: (black) 17 214, (red) 16 517, and (blue) 15 503 cm^{-1}. Spectra are offset vertically for clarity.

comprising peaks A1−A16, with a typical peak spacing of ∼180 cm^{-1}. A second progression of peaks a5−a12 is visible with much smaller intensity. It has the same peak spacing as the main progression but is offset ∼80 cm^{-1} higher. The three different traces in Figure 3 illustrate that the relative intensities of peaks drop dramatically at low eKE (i.e., at eBE close to the photon energy), where the resolution is highest. To maintain a balance between signal and resolution, the peak assignments are taken from spectra with eKE ∼500 cm^{-1}, giving typical peak widths of 15 cm^{-1} fwhm in this region.

dx.doi.org/10.1021/ja502713v | J. Am. Chem. Soc. 2014, 136, 7159−7168

The overview spectra also show much stronger photoelectron signal at higher eBE, ~17 000−20 000 cm^{-1} (band B). Much of the signal is not fully resolved, but two peak progressions are visible with a spacing of 95 cm^{-1}, one from ~17 000 to 18 000 cm^{-1} and another from ~18 500 to 19 500 cm^{-1}. As the region in the higher-eBE progression is highly congested, high-resolution spectra were obtained only for the low-eBE portion of band B (Figure 4). The progression

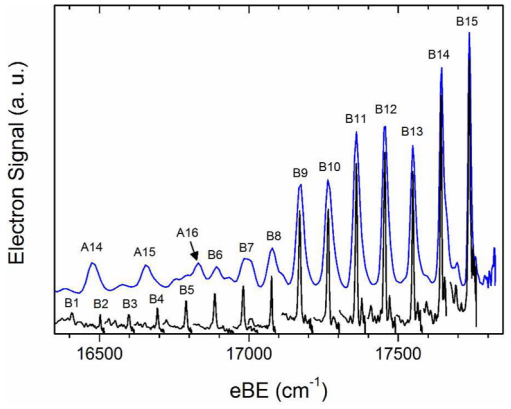

Figure 4. SEVI spectra of the low-eBE portion of the C_{2v} Ti_2O_4 PE spectrum (band B). The overview spectrum (blue, at photon energy of 17 824 cm^{-1}) is offset vertically from the high-resolution segments (black).

observed in the overview spectra is still the dominant feature, comprising peaks B1−B15 with a typical peak spacing of 95 cm^{-1}. Peak intensities do not disappear near threshold, resulting in peak widths as narrow as 7 cm^{-1} at eKEs around 30 cm^{-1}. Weak features other than the main B1−B15 progression are also visible above 17 300 cm^{-1}, though poor signal-to-noise and spectral congestion prevents clear peak labeling or assignments.

Peak positions, PADs, and assignments for $Ti_2O_4^-$ high-resolution SEVI spectra are listed in Table S1 in Supporting Information. The value of β describing the PAD is a function of eKE, which is not a constant for a given transition in this experiment. At large eKE (1000−4000 cm^{-1}), the anisotropy parameter of all transitions is unambiguously positive ($\beta > 0.6$), but at eKE < 500 cm^{-1}, the value of β for a given well-resolved peak can be binned as either $0 < \beta < 0.2$ or $0.3 < \beta < 1$ (Figure S1, Supporting Information). These two categories are labeled a- and b-PADs. The PAD is characterized by a β-value of a for peaks B8−B15, while peaks A3−A14 and a8−a12 had a b-PAD. All other peaks had too little signal for an accurate determination.

In contrast to the extended progressions seen in the $Ti_2O_4^-$ spectra, the $Zr_2O_4^-$ spectra show a strong onset (peak A) and no immediately dominant peak progression, though there are several peaks with strong intensity (Figure 5). Significant structure extends for only ~2000 cm^{-1} beyond the band onset, and peak widths as narrow as 4 cm^{-1} are obtained. A very weak progression is also present close to the band onset (Figure 5 inset), comprising peaks a1−a7, with a typical peak spacing of 95 cm^{-1}. In contrast with all other assigned peaks, for which the PAD is b, these have an a-PAD. Peak positions, PADs, and assignments for $Zr_2O_4^-$ spectra are listed in Table S2 in Supporting Information.

4.2. Calculations. Calculated relative energies for anionic and neutral isomers of Ti_2O_4 and Zr_2O_4 are summarized in Table 1. Adiabatic detachment energies (ADE), vertical detachment energies (VDE), and reorganization energies are also listed. These values are defined as the difference between anion and neutral energies at their respective minima, the difference at anion geometries, or the difference between VDE and ADE, respectively. These values are taken from the benchmark CCSD(T)/CBS calculations by Li and Dixon,[45,48] who found that the different isomers are only a few kilocalories per mole apart in energy. This difference is smaller than the expected error of BP86 and other density functionals,[62] hence the values from their papers are used here rather than

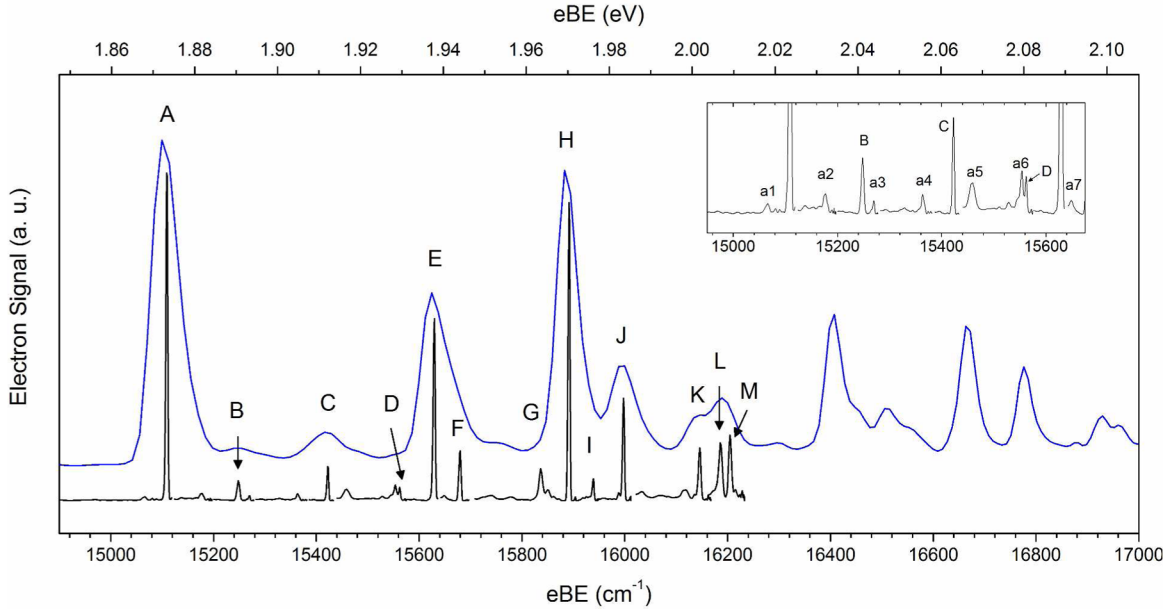

Figure 5. SEVI spectra of Zr_2O_4. The overview spectrum (blue, at photon energy of 17 682 cm^{-1}) is offset vertically from the high-resolution segments (black). (Inset) Weak but reproducible peaks between 15 000 and 15 700 cm^{-1}.

dx.doi.org/10.1021/ja502713v | J. Am. Chem. Soc. 2014, 136, 7159−7168

Table 1. Calculated Energetics of Anion $M_2O_4^-$ (M = Ti, Zr) Isomers and Selected Vibrational Frequencies of Neutral Species[a]

	Ti_2O_4			Zr_2O_4		
	C_{2h}	C_{2v}	C_{3v}	C_{2h}	C_{2v}	C_{3v}
relative anion energy, kcal/mol	1.6[b]	0.0[b]	6.7[b]	4.8[c]	2.5[c]	0.0[c]
relative neutral energy, kcal/mol	0.0[b]	5.5[b]	12.8[b]	0.0[c]	6.2[c]	6.4[c]
ADE,[d] eV	1.64	1.95	1.98	1.42	1.79	1.91
VDE,[d] eV	2.22	2.32	2.13	1.62	2.15	2.12
reorganization energy, eV	0.58	0.37	0.15	0.20	0.36	0.21
ν_1, cm^{-1}	991	1002	997	871	874	856
ν_2, cm^{-1}	721	719	832	630	636	740
ν_3, cm^{-1}	404	409	561	303	322	506
ν_4, cm^{-1}	200	315	400	159	255	297
ν_5, cm^{-1}		94			97	

[a]Energetics are from CCSD(T)/CBS calculations by Li and Dixon,[45,48] and frequencies are from this work. [b]From ref 45. [c]From ref 48. [d]ADE, adiabatic detachment energy; VDE, vertical detachment energy.

recalculated with DFT. Calculated bond lengths (Tables S3–S5, Supporting Information) are consistent with the simple picture (Figure 1) of bridging oxo and terminal oxo ligands with single and double bonding to the respective metal centers. For all isomers, the assigned M—O bond lengths are consistently ~0.2 Å longer than the corresponding M═O bond lengths. The most significant change in geometry with differing charge states is the out-of-plane terminal oxo angle for the C_{2h} and C_{2v} isomers; this feature is discussed in further detail in section 6.2.

Selected vibrational frequencies are also listed in Table 1. Only totally symmetric vibrational modes are listed, as these are typically the modes that dominate Franck–Condon activity. The C_{2h} and C_{3v} isomers have four totally symmetric modes (a_g and a_1) each, while the C_{2v} isomer has five totally symmetric (a_1) modes. A full listing is given in Tables S3–S5 of Supporting Information for the geometries and vibrational frequencies of all three symmetries and both charge states of the two M_2O_4 species. All neutrals are closed-shell species, and all anions have a singly occupied molecular orbital (SOMO) of the totally symmetric representation of the respective point group. The anion SOMO and major geometry changes are shown in Figure 6.

Franck–Condon simulations are shown in Figure 7 for photodetachment of all three isomers of $Ti_2O_4^-$ and $Zr_2O_4^-$. Each of the three isomers has a distinct FC profile, which changes somewhat depending on the metal atom. The C_{2h} isomer exhibits an extended progression in the lowest-frequency totally symmetric mode, the ν_4 mode. The predicted peak spacing is 200 and 159 cm^{-1} for Ti and Zr, respectively. The band progression is calculated to extend 6000 cm^{-1} for Ti_2O_4 but only 1500 cm^{-1} for Zr_2O_4. The C_{2v} isomer also has a large progression in its lowest-frequency totally symmetric mode, the ν_5 mode, with a predicted peak spacing of 94 and 97 cm^{-1} for Ti and Zr. However, other modes are also predicted to be FC-active, especially the ν_3 mode, resulting in a highly congested spectrum starting from ~1500 cm^{-1} above the vibrational origin and extending at least 6000 cm^{-1}. Displacement vectors for the most FC-active C_{2h} and C_{2v} modes are illustrated in Figure 6.

In contrast, the FC simulation of the C_{3v} isomer is not dominated by activity in any one particular mode. The vibrational origin is strong, and appreciable FC activity is predicted in all the totally symmetric modes (with the exception of ν_3 in Ti_2O_4). There is also some minor even quanta excitation in the nontotally symmetric ν_8 mode, which corresponds to the terminal oxygen wagging motion, owing to the large change in vibrational frequency between anion and neutral species (Table S5, Supporting Information).

It is also of interest to consider the infrared spectra of the various anion and neutral isomers. For this purpose, simulated vibrational spectra are displayed in Figure S2 (Supporting Information).

5. ANALYSIS

5.1. Assignment of $Ti_2O_4^-$ Spectra. Bands A and B have different PADs, suggesting that they correspond to two different photodetachment transitions rather than two vibrational progressions within the same electronic transition. Different experimental conditions at identical photodetachment energies can also change the relative intensities of the two bands (Figure S3, Supporting Information), though the correlation between conditions used and band strengths is

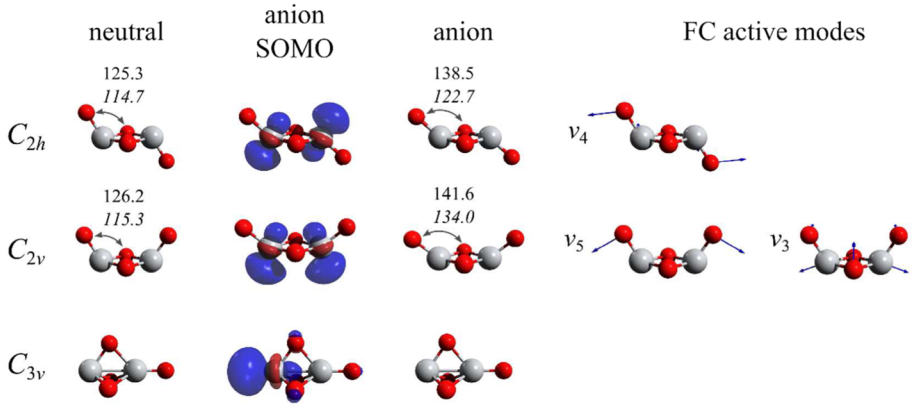

Figure 6. Major geometry and electronic changes between the anion and neutral species, along with the most active Franck–Condon modes. The M—M═O bond angle is highlighted in the C_{2v} and C_{2h} isomers, as this is the dominant geometry change in those Ti_2O_4 (plain) and Zr_2O_4 (italic) isomers. As the qualitative geometry changes, anion singly occupied molecular orbital (SOMO) and normal modes are similar between the two metals; only those for Ti_2O_4 at the BP86/LANL2TZ level are displayed.

dx.doi.org/10.1021/ja502713v | J. Am. Chem. Soc. 2014, 136, 7159–7168

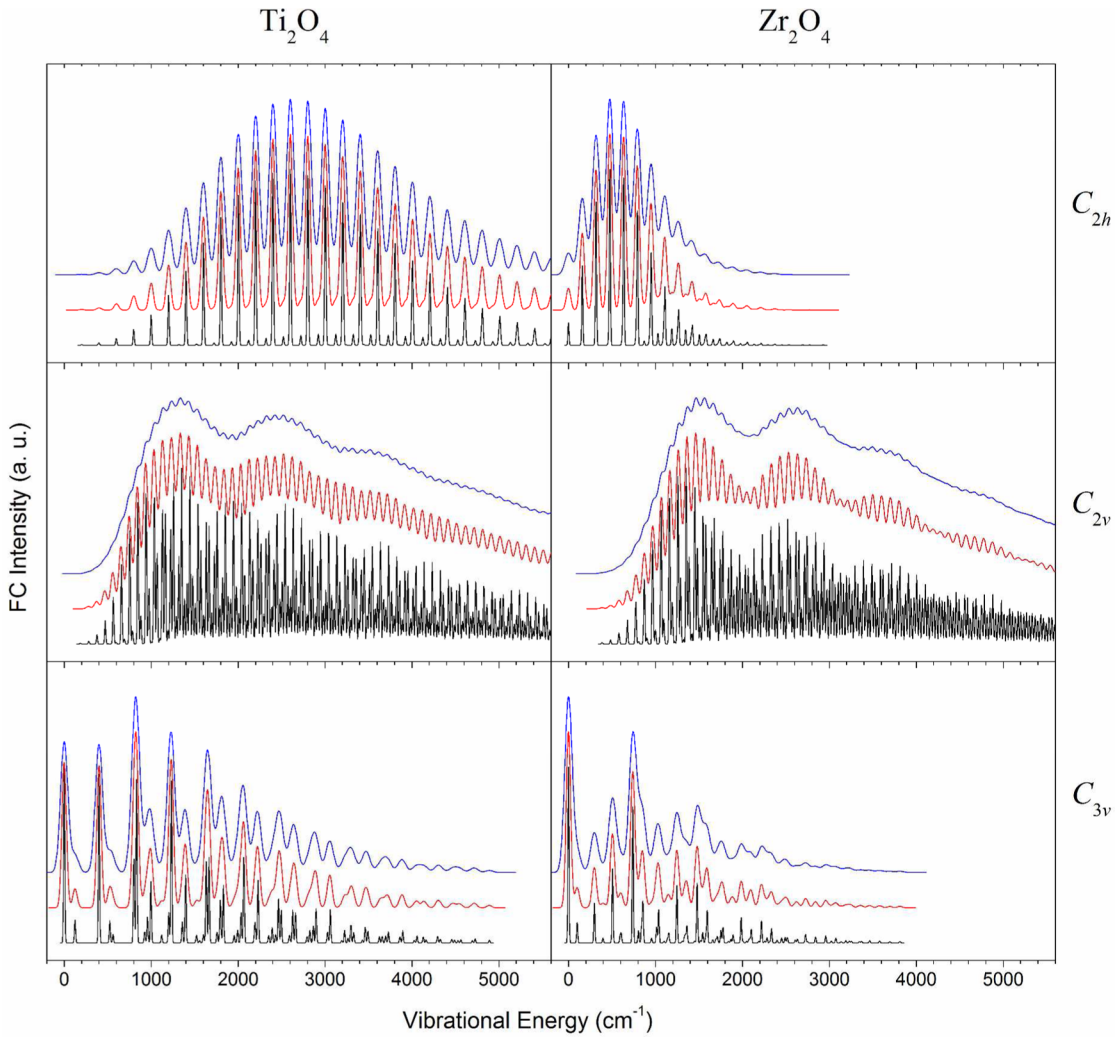

Figure 7. Franck–Condon simulations of photodetachment of $M_2O_4^-$ for C_{2h}, C_{2v}, and C_{3v} isomers with M = Ti, Zr. Simulations are offset vertically and broadened by Gaussian distributions with fwhm of (black) 15, (red) 60, and (blue) 100 cm^{-1}.

not clear. The two bands have peak progressions with different spacings, ruling out detachment from two anion states to the same neutral state. While they could arise from photodetachment to two close-lying neutral states from the same anion state, theoretical calculations do not support the existence of very low-lying states for any of the neutral isomers, all of which are closed-shell species.[45] The two bands are most reasonably assigned to photodetachment from two different anion isomers, each going to a neutral isomer of the same molecular symmetry and overall structure.

The two bands can be assigned by comparing the observed peak spacings and intensity distributions to calculations. Band A exhibits an extended progression in a vibrational mode with a frequency of ~180 cm^{-1}, while the clearest progression in band B involves a mode with a frequency of ~95 cm^{-1}. These correspond well to the calculated frequencies of ν_4 mode of neutral C_{2h} isomer (200 cm^{-1}) and ν_5 mode of C_{2v} isomer (94 cm^{-1}) (see Table 1). By comparison, the ν_4 modes of C_{2v} and C_{3v} isomers have calculated frequencies of 315 and 400 cm^{-1}, respectively, and do not match the observed vibrational spacing. While Δv = even transitions are possible for nontotally symmetric modes, such progressions are often weak; the large FC activity is indicative of strong activity in fully FC-allowed modes. The vibrational spacing is consistent with bands A and B corresponding to photodetachment of C_{2h} and C_{2v} isomers, respectively, of $Ti_2O_4^-$.

The FC simulations in Figure 7 confirm this assignment. The C_{2h} ν_4 and C_{2v} ν_5 modes are calculated to be the most FC-active modes for the respective isomers, matching the assigned vibrational activity on the basis of peak spacing. The FC envelopes for both isomers are >4000 cm^{-1} wide, consistent with the observation that both bands are extended >3000 cm^{-1}. There is also significant simulated FC activity in other modes of the C_{2v} isomer. Due to overlapping contributions from multiple modes, this activity appears as a bimodal distribution with peak spacing approximating that of the ν_5 frequency, as seen in the red and blue traces in the C_{2v} simulation in Figure 7. This bimodal appearance is also seen in the experimental spectra, most clearly in the black and red traces in Figure 2. The C_{3v} simulation, in contrast, has a strong vibrational onset and FC activity is more distributed among the various FC-active modes, completely unlike that observed for bands A and B. The much stronger signal associated with band B suggests that the C_{2v} anion isomer is more stable than the C_{2h} isomer, a point discussed further in section 6.1.

The eKE-dependent intensities in bands A and B, most apparent in Figures 3 and 4, are also consistent with this assignment. The peak intensities at low eKE drop off for the

dx.doi.org/10.1021/ja502713v | J. Am. Chem. Soc. 2014, 136, 7159–7168

peaks in band A but not in band B. These results can be understood with reference to the Wigner threshold law[55] as applied to the photodetachment cross section σ for low-energy electrons, $\sigma \propto (\mathrm{eKE})^{l+1/2}$, where l is the orbital angular momentum of the outgoing electron.

Our results imply that the partial waves contributing to photodetachment near threshold differ for the two bands, with more s-wave ($l = 0$) detachment for band B and more p-wave ($l = 1$) or higher-order detachment for band A. The SOMO shown in Figure 6 for the C_{2h} isomer has g symmetry with respect to inversion through the center of symmetry. As shown by Reed et al.,[63] s-wave photodetachment from such an orbital is symmetry-forbidden, resulting in eKE-dependent intensities of the type seen in band A. The C_{2v} isomer has no center of symmetry, so this selection rule does not apply, and s-wave detachment is fully allowed.

As the C_{2v} and C_{2h} isomers are only a few kilocalories per mole apart in energy while the vibrational progressions are highly extended, it is worth considering whether any spectral features can be attributed to isomerization. However, B3LYP calculations show that the barrier to isomerization along the oxygen wagging motion connecting those isomers is at least 0.70 eV.[64] While higher-eBE portions of the spectra may well have contributions from motion near the barrier, the assigned features at lower eBE can be attributed solely to one isomer or the other.

Although the experimental data for the $Ti_2O_4^-$ SEVI spectra are consistent with the lower-resolution PE spectrum reported by Zhai and Wang,[29] we assign the main feature to the C_{2v} isomer while they assigned it to the C_{3v} isomer. The previous PE study had no vibrationally resolved structure, so the assignments were made by comparison of the experimental electronic state energies to those obtained by theoretical calculations,[29,41] which had predicted a C_{3v} anion minimum. The calculations used, however, were made with a relatively low-level local DFT method and a plane-wave basis set.[38] Subsequent DFT calculations have found either a C_{2h} or C_{2v} isomer to be the $Ti_2O_4^-$ minimum.[40,45]

In addition to enabling identification of the anion isomers, the well-resolved vibrational structure allows us to determine vibrational frequencies of the neutral C_{2v} and C_{2h} isomers of Ti_2O_4. The primary structure in band A corresponds to a progression in the ν_4 mode in C_{2h} Ti_2O_4, with a vibrational frequency of ~180 cm^{-1}. By fitting the A1−A16 progression to the lowest-order anharmonic oscillator and assuming A1 corresponds to the vibrational origin, we obtain a ν_4 fundamental of 185(4) cm^{-1} and harmonic frequency ω_4 = 186(4) cm^{-1}. If A1 is not the origin, the frequencies will be slightly larger due to the anharmonicity. The a5−a12 progression corresponds to another progression in the same ν_4 mode but with one quantum in another totally symmetric mode. The onset of this progression is even more difficult to determine than that of the A1−A16 progression due to the weak signal. If peak a5 is offset from peaks A1, A2, A3, or A4 by one quantum in a different mode, the fundamental of that mode would be 823, 637, 455, or 271 cm^{-1}, respectively. When these values are compared to the calculated frequencies of the totally symmetric modes, the best agreement comes with 455 cm^{-1} for the ν_3 mode. Peaks a5−a12 are then assigned to the $3_0^1 4_0^n$ progression; a similar analysis for the 4_0^n progression gives ν_3 = 458(5) cm^{-1}.

The resolved vibrational structure in the C_{2v} band is dominated by the ~95 cm^{-1} 5_0^n progression. Although the origin is similarly not well-established, there is much less anharmonicity compared to the C_{2h} 4_0^n progression. By similar fitting, we obtain both the vibrational fundamental and harmonic frequencies $\nu_4 = \omega_4$ = 95(2) cm^{-1}. Note that in the high-resolution SEVI spectra, the intensities of this progression do not increase smoothly, which may be due to contributions from unresolved additional structure. However, no other evidence of such structure is seen even at a resolution of ~7 cm^{-1}.

5.2. Assignment of $Zr_2O_4^-$ Spectra. The SEVI spectra of $Zr_2O_4^-$ also show two overlapped bands, one considerably more intense than the other, with differing PADs and characteristic peak spacings. The same reasoning that was applied to $Ti_2O_4^-$ suggests that these bands correspond to transitions originating from two anion isomers. As with $Ti_2O_4^-$, the vibrational structure in the SEVI spectra readily allows us to assign each band to a particular isomer. The main band, peaks A−M, is not dominated by a single peak progression and has a strong vibrational origin, consistent with the FC simulation for photodetachment from the C_{3v} isomer. Moreover, within 1000 cm^{-1} of the vibrational origin, significant peaks are predicted for the 8_0^2, 4_0^1, 3_0^1, 2_0^1, and 1_0^1 transitions at 100, 29, 506, 740, and 856 cm^{-1} above the origin. These predictions are in good agreement with the experimental positions and intensities of peaks B, C, E, H, and J (Table S2, Supporting Information) and are assigned, respectively. By appropriate combinations, peak D is assigned as the $4_0^1 8_0^2$ transition, peak K as 3_0^2, and peak M as $2_0^1 4_0^1$. The observed vibrational structure allows us to obtain numerous vibrational fundamentals of C_{3v} Zr_2O_4 (Table 2).

Table 2. Summary of Experimental Detachment Energies of Anions and Vibrational Frequencies of Neutral M_2O_4 Isomers

	Ti_2O_4		Zr_2O_4	
	C_{2h}	C_{2v}	C_{2v}	C_{3v}
ADE,[a] eV	1.752(1)[b]	2.035(1)[b]	1.8681(5)[b]	1.8733(2)
VDE,[a] eV	2.1(1)	2.28(3)	1.92(6)	2.00(3)
ν_1, cm^{-1}				888(2)
ν_2, cm^{-1}				782(2)
ν_3, cm^{-1}	458(5)			520(2)
ν_4, cm^{-1}	185(4)			313(2)
ν_5, cm^{-1}		95(2)	95(10)	
ν_8, cm^{-1}				70(2)

[a]ADE, adiabatic detachment energy; VDE, vertical detachment energy. [b]Upper limits.

The fundamental of the nontotally symmetric ν_8 mode is not observed. However, its intermode anharmonicity is small; that is, peak D is offset from the origin exactly as the combination of peaks B and C. We assume that the intramode anharmonicity is similarly small, and we give the fundamental frequency as half that of $2\nu_8$.

The weak band, peaks a1−a7, comprises a single ~95 cm^{-1} progression. The appearance of this band suggests it should be assigned to photodetachment of the C_{2v} isomer, for which an extended 5_0^n progression with a peak spacing of 97 cm^{-1} peak spacing is predicted. The lowest-frequency a_g mode of C_{2h} Zr_2O_4 is calculated to have a frequency of 159 cm^{-1} and is not likely to correspond to the observed band. The low signal of this band makes a precise determination of the ν_5 frequency

dx.doi.org/10.1021/ja502713v | J. Am. Chem. Soc. 2014, 136, 7159−7168

more difficult, and we conservatively give a value of 95(10) cm^{-1}.

5.3. Adiabatic and Vertical Detachment Energies. Adiabatic detachment energies (ADE) are experimentally given for each anion isomer by the position of the vibrational origin of the corresponding band in the SEVI spectrum. For $Ti_2O_4^-$, the lowest energy transitions observed for bands A and B (peaks A1 and B1) occur at 1.752(1) and 2.035(1) eV, respectively. Since these bands are both quite extended, it is possible that these peaks are not the vibrational origins, in which case these energies are upper bounds for the ADEs of the C_{2h} and C_{2v} isomers of $Ti_2O_4^-$. The vibrational origin of the main band (peak A) is clear and well-resolved in the SEVI spectrum of $Zr_2O_4^-$, yielding an ADE of 1.8733(2) eV for the C_{3v} isomer. The weak band has peak a1 as the first resolved feature, giving an upper bound of 1.8681(5) eV for the ADE of the $Zr_2O_4^-$ C_{2v} isomer. As this band is calculated to have an extended FC progression while its intensity is experimentally very small, the true ADE is likely to be smaller.

It is also useful to extract vertical detachment energies (VDE) from our spectra for comparison with calculations and lower-resolution photoelectron spectra. We take the experimental VDEs to be the center of gravity of each band. For $Ti_2O_4^-$, the signal in band A diminishes close to threshold and the high-eBE portion overlaps with the much more intense band B. Hence only a rough estimate can be given of 2.1(1) eV for the VDE of band A (C_{2h}), compared to a more precise value of 2.28(3) eV for band B (C_{2v}). A similar procedure for $Zr_2O_4^-$ yields VDEs of 1.92(6) and 2.00(3) eV for the C_{2v} and C_{3v} isomers, respectively. The small differences between VDEs for the various isomers is consistent with previous electronic structure calculations[38,45,48] and points to the difficulties of using these quantities as the sole basis for assigning features in photoelectron spectra to particular isomers.

6. DISCUSSION

6.1. Isomers and Energetics. Vibrationally resolved PE spectra obtained by SEVI show that the dominant photodetachment signal is from the C_{2v} and C_{3v} isomers of $Ti_2O_4^-$ and $Zr_2O_4^-$, respectively. As the detached electrons for all three isomers come from a metal-centered d-orbital SOMO (Figure 6), one can assume that the different isomers have a comparable photodetachment cross-section (so long as they are not too close to the detachment threshold) and thus that the observed photoelectron signal corresponds to the relative populations of the two isomers. The ions have been cooled in a clustering channel in the laser ablation source and then further cooled in the cryogenic ion trap. This combination is likely to favor production of the most stable anion isomers. It thus appears that the lowest-energy anion isomers are the C_{2v} structure for $Ti_2O_4^-$ and the C_{3v} structure for $Zr_2O_4^-$. On the basis of our assignment of the weak bands for the two clusters, the next highest energy isomers are the C_{2h} and C_{2v} structures for $Ti_2O_4^-$ and $Zr_2O_4^-$, respectively. This energy ordering agrees with the calculations by Li and Dixon[45,48] (see Table 1).

The weaker band is more prominent in $Ti_2O_4^-$ than in $Zr_2O_4^-$, suggesting a larger population for the higher energy anion isomer; this result may reflect less efficient cooling of $Ti_2O_4^-$ by pure He in the ion trap,[53] compared to the H_2/He mixture used for $Zr_2O_4^-$. The $Ti_2O_4^-$ ions appear to have minimal vibrational excitation, as no sequence or hot bands are observed, but inefficient cooling may still affect the isomer distribution prior to total quenching of vibrational energy.

Neutral Ti_2O_4 and Zr_2O_4 have been studied by IR spectroscopy in a rare gas matrix.[36] On the basis of the vibrational structure observed with varied amounts of ^{18}O labeling, both Zr_2O_4 and Ti_2O_4 were determined to have a C_{2h} ground state in a matrix. For example, without isotope labeling, only a single peak was seen between 850 and 900 cm^{-1}, as opposed to a doublet that would be present for C_{2v} isomers (see Figure S2 in Supporting Information). With partial isotope labeling, however, both the symmetric and antisymmetric stretch modes are observed due to the breaking of symmetry. Most theoretical calculations also predict a C_{2h} isomer for the neutral M_2O_4 species. Hence, it appears that the energy ordering of the anion and neutral isomers is different, which is again consistent with electronic structure calculations.[38,45,48]

Although we can identify the most stable anion isomers based on the relative signal intensities, the two bands seen in the SEVI spectra for each species do not correspond to photodetachment to a common neutral isomer, as shown in Figure 8; the energetics here are from the calculations of Li and Dixon.[45,48] In fact, neither band in $Zr_2O_4^-$ accesses the C_{2h} ground-state neutral isomer. As a result, one cannot derive energy differences between the anion (or neutral) isomers from the SEVI spectra alone. Nonetheless, since the relative energy ordering of the two lowest anion isomers and their ADE values are known, one can put limits on the energy splitting of the corresponding neutral isomers. In $Ti_2O_4^-$, if one were to assume the C_{2h} and C_{2v} isomers to be degenerate, then from the ADE values reported in Table 2, the neutral C_{2v} isomer lies 0.283 eV above the C_{2h} isomer. However, since the anion C_{2v} isomer is lower in energy, this value is an upper bound to the neutral splitting, consistent with the calculated splitting of 0.24 eV. A similar analysis for $Zr_2O_4^-$ would place an upper bound of only 0.005 eV between the C_{2v} and C_{3v} neutral isomers, which is smaller than the calculated splitting of 0.009 eV. The analysis in this case is complicated by assignment of the ADE for the C_{2v} isomer of $Zr_2O_4^-$; as described in section 5.2, this ADE is likely to be smaller than the upper bound we have assigned, and a smaller value would increase the neutral isomer energy difference.

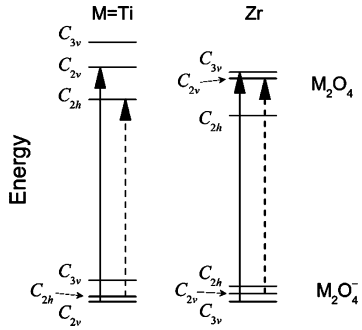

Figure 8. Energy level diagram of the various isomers and charge states of Ti_2O_4 and Zr_2O_4. Energies are from CCSD(T) calculations by Li and Dixon.[45,48] The full arrow highlights the primary observed photodetachment channel in this work, while the dashed arrow is a minor component.

The energy resolution of the SEVI spectra shown here is comparable to the highest-resolution results achieved in IRPD spectroscopy of metal oxide clusters,[12] raising the question of which method is more suited for structural characterization of the two species. As indicated by the simulated IR spectra in

dx.doi.org/10.1021/ja502713v | J. Am. Chem. Soc. 2014, 136, 7159−7168

Figure S2 (Supporting Information), there are distinct differences in the IR spectra of the various isomers as well. Both methods could be successfully used to identify the $M_2O_4^-$ structures but in complementary ways. In particular, most of the major features in the IR spectra are due to various M—O and M═O stretching modes. In comparison, the main progressions in the C_{2v} and C_{2h} SEVI spectra are due to much lower frequency terminal oxygen wagging modes that are barely active in the IR spectra, while the IR-active M—O and M═O modes only have significant activity in the SEVI spectra for the C_{3v} isomer. Also, gas-phase IR spectra of size-selected neutral metal oxide clusters are challenging to obtain, whereas the SEVI experiment yields these vibrational frequencies directly. Conversely, IRPD spectra are routinely obtained for anions, while SEVI can only give vibrational information on anions through the observation of hot bands.

6.2. Geometry and Franck–Condon Activity. Earlier interpretations of the PE spectra of $(TiO_2)_n$ clusters attributed the broad unresolved spectra to extended FC activity. The FC activity, in turn, was attributed to photodetachment of an electron from the localized SOMO in the anion, resulting in a large geometry change, as detachment from a delocalized orbital would perturb the geometry less.[13,29] We reconsider this interpretation with information gained from the present study.

The specifics of FC activity differ for the various isomers. The C_{2v} and C_{2h} isomers have a structural motif with a M_2O_2 ring and two terminal oxygen atoms. The anion SOMO for both isomers distorts the angle of the out-of-plane terminal oxygen atoms. Since most of the electron density is out of the M_2O_2 plane, the resulting electrostatic repulsion with the oxygen atoms preferentially distorts the terminal oxygen atoms to be more coplanar with the M_2O_2 ring. Although the SOMO is nominally a nonbonding orbital, the resulting change in geometry leads to a large reorganization energy. Our calculations predict a 15.4° change in the Ti—Ti═O bond angle for the Ti_2O_4 C_{2v} isomer, and the C_{2h} isomer and Zr_2O_4 species have similar calculated changes in geometry (Figure 6). The most FC-active modes should correspond to the symmetric bend of the terminal oxygen atoms, which would be ν_4 mode of C_{2h} isomer and ν_5 mode of C_{2v} isomer, with some contribution from ν_3 mode as well. The C_{3v} isomer, in contrast, has the additional anion electron localized on one atom. The molecular framework is more rigid near the SOMO than in the other isomers, and only minor changes in geometry are immediately obvious. The reorganization energy is consequently smaller than the other isomers, with the exception of C_{2h} Zr_2O_4. The geometry changes are also not well-described by any one vibrational mode, and thus more if not all of the totally symmetric modes are expected to be FC-active.

Compared with the expected FC-active modes on the basis of the anion SOMO and geometry changes, the calculated FC simulations are in good agreement. The M_2O_4 C_{2h} simulations exhibit a broad progression in the ν_4 mode, the C_{2v} simulations have large progressions in the ν_3 and ν_5 modes, and the C_{3v} simulations have less FC activity overall but all the totally symmetric modes contribute. Relative to the other isomers, the vibrational origin is far more prominent in the C_{3v} isomer spectra. It thus appears that charge localization cannot be used as the sole criterion for rationalizing the width of PE spectral features from unresolved vibrational activity. Calculated reorganization energies can provide guides for the width of the FC envelope, but in this case a proper vibrational analysis is required to definitively assign the PE features.

7. CONCLUSION

The structural isomers of $Ti_2O_4^-$ and $Zr_2O_4^-$ have been determined by comparing calculated vibrational frequencies and Franck–Condon profiles with high-resolution anion photoelectron spectra obtained by SEVI and cryogenic ion cooling. The ground $Ti_2O_4^-$ isomer is C_{2v} and the next lowest-lying isomer is C_{2h}, while the neutral isomers are reversed in order of energy. In contrast, $Zr_2O_4^-$ is observed as the C_{3v} isomer, with only trace quantities of the C_{2v} isomer. Due to the extended vibrational progressions in C_{2h} and C_{2v} isomers, the ADE is definitively identified only for C_{3v} $Zr_2O_4^-$, while upper bounds have been put on the $Zr_2O_4^-$ C_{2v} isomer as well as the $Ti_2O_4^-$ C_{2v} and C_{2h} isomers. Various vibrational frequencies of the neutral species have been determined. The energy ordering of the anion isomers disagrees with some theoretical studies but bolsters the conclusions of previously reported sophisticated ab initio calculations by Li and Dixon,[45,48] giving experimental evidence in favor of their calculated isomer energy ordering.

Even the relatively simple $(MO_2)_2$ species studied have multiple isomers close in energy that have proven a challenge to describe computationally. Moreover, few techniques are well-suited for experimentally determining the structures and energetics of size-selected metal oxide clusters. Anion PE spectroscopy can obtain detachment energies, which can be compared with calculations, but only in favorable circumstances has vibrational structure been resolved and used to corroborate the assignments. The addition of SEVI and ion cooling to anion PE spectroscopy allows for vibrational resolution of many more systems, resulting in more conclusive assignments of structures, energies, and vibrational frequencies.

■ ASSOCIATED CONTENT

Ⓢ Supporting Information

Five tables and three figures showing full listing of experimental SEVI peak positions and assignments, calculated geometries and vibrational frequencies at the BP86/LANL2TZ level for all species considered, plots of β as a function of eKE and isomer, simulated IR spectra of all species, and overview spectra demonstrating that relative band intensities depend on experimental conditions and have different characteristic PADs. This material is available free of charge via the Internet at http://pubs.acs.org.

■ AUTHOR INFORMATION

Corresponding Author

dneumark@berkeley.edu

Notes

The authors declare no competing financial interest.

■ ACKNOWLEDGMENTS

This work was funded by the Air Force Office of Scientific Research under Grant FA9550-12-1-0160 and the Defense University Research Instrumentation Program under Grant FA9550-11-1-0330. M.L.W. thanks the National Science Foundation for a graduate research fellowship.

■ REFERENCES

(1) Tanabe, K. *Mater. Chem. Phys.* **1985**, *13*, 347.
(2) Greenwood, N. N.; Earnshaw, A. *Chemistry of the Elements*, 2nd ed.; Elsevier: Oxford, U.K., 1998.
(3) Salem, I. *Catal. Rev.* **2003**, *45*, 205.
(4) Fujishima, A.; Honda, K. *Nature* **1972**, *238*, 37.

(5) Fujishima, A.; Zhang, X.; Tryk, D. A. *Surf. Sci. Rep.* **2008**, *63*, 515.
(6) Diebold, U. *Surf. Sci. Rep.* **2003**, *48*, 53.
(7) Henrich, V. E.; Cox, P. A. *The Surface Science of Metal Oxides*; University Press: Cambridge, U.K., 1994.
(8) Castleman, A. W. *Catal. Lett.* **2011**, *141*, 1243.
(9) Armentrout, P. B. *Annu. Rev. Phys. Chem.* **2001**, *52*, 423.
(10) Böhme, D. K.; Schwarz, H. *Angew. Chem., Int. Ed.* **2005**, *44*, 2336.
(11) Haertelt, M.; Fielicke, A.; Meijer, G.; Kwapien, K.; Sierka, M.; Sauer, J. *Phys. Chem. Chem. Phys.* **2012**, *14*, 2849.
(12) Asmis, K. R. *Phys. Chem. Chem. Phys.* **2012**, *14*, 9270.
(13) Zhai, H.-J.; Wang, L.-S. *Chem. Phys. Lett.* **2010**, *500*, 185.
(14) Mann, J. E.; Mayhall, N. J.; Jarrold, C. C. *Chem. Phys. Lett.* **2012**, *525*−*526*, 1.
(15) Gong, Y.; Zhou, M.; Andrews, L. *Chem. Rev.* **2009**, *109*, 6765.
(16) Wang, L.-S. In *Photoionization and Photodetachment*; Ng, C. Y., Ed.; World Scientific: Singapore, 2000; Vol. *10*.
(17) Collaboration: Authors and editors of the volumes III/17G-41D. Titanium oxide (TiO_2): energy gap, further interband transitions in rutile. In *Volume 41, Semiconductors: Subvolume D, Non-Tetrahedrally Bonded Binary Compounds II*; Madelung, O., Ed.; Landolt-Börnstein Numerical Data and Functional Relationships in Science and Technology, New Series: Group III, Condensed Matter; Springer: Berlin and Heidelberg, Germany, 2000; Vol. *41D*.
(18) Seehra, M. S.; Wijn, H. P. J. Oxides of 4d and 5d transition elements. In *Volume 27, Magnetic Properties of Non-Metallic Inorganic Compounds Based on Transition Elements: Subvolume G, Various Other Oxides*; Wijn, H. P. J., Ed.; Landolt-Börnstein Numerical Data and Functional Relationships in Science and Technology, New Series: Group III, Condensed Matter; Springer: Berlin and Heidelberg, Germany, 1992; Vol. *27G*.
(19) Asmis, K. R.; Sauer, J. *Mass Spectrom. Rev.* **2007**, *26*, 542.
(20) Johnson, G. E.; Mitrić, R.; Tyo, E. C.; Bonačić-Koutecký, V.; Castleman, A. W. *J. Am. Chem. Soc.* **2008**, *130*, 13912.
(21) Tyo, E. C.; Noler, M.; Mitric, R.; Bonacic-Koutecky, V.; Castleman, A. W., Jr. *Phys. Chem. Chem. Phys.* **2011**, *13*, 4243.
(22) Harvey, J. N.; Diefenbach, M.; Schröder, D.; Schwarz, H. *Int. J. Mass. Spectrom.* **1999**, *182*−*183*, 85.
(23) Ma, J.-B.; Xu, B.; Meng, J.-H.; Wu, X.-N.; Ding, X.-L.; Li, X.-N.; He, S.-G. *J. Am. Chem. Soc.* **2013**, *135*, 2991.
(24) Matsuda, Y.; Shin, D. N.; Bernstein, E. R. *J. Chem. Phys.* **2004**, *120*, 4142.
(25) Matsuda, Y.; Bernstein, E. R. *J. Phys. Chem. A* **2005**, *109*, 314.
(26) von Helden, G.; Kirilyuk, A.; van Heijnsbergen, D.; Sartakov, B.; Duncan, M. A.; Meijer, G. *Chem. Phys.* **2000**, *262*, 31.
(27) Demyk, K.; van Heijnsbergen, D.; von Helden, G.; Meijer, G. *Astron. Astrophys.* **2004**, *420*, 547.
(28) Wu, H.; Wang, L.-S. *J. Chem. Phys.* **1997**, *107*, 8221.
(29) Zhai, H.-J.; Wang, L.-S. *J. Am. Chem. Soc.* **2007**, *129*, 3022.
(30) Chertihin, G. V.; Andrews, L. *J. Phys. Chem.* **1995**, *99*, 6356.
(31) Brugh, D. J.; Suenram, R. D.; Stevens, W. J. *J. Chem. Phys.* **1999**, *111*, 3526.
(32) Brünken, S.; Müller, H. S. P.; Menten, K. M.; McCarthy, M. C.; Thaddeus, P. *Astrophys. J.* **2008**, *676*.
(33) Zhuang, X.; Le, A.; Steimle, T. C.; Nagarajan, R.; Gupta, V.; Maier, J. P. *Phys. Chem. Chem. Phys.* **2010**, *12*, 15018.
(34) Le, A.; Steimle, T. C.; Gupta, V.; Rice, C. A.; Maier, J. P.; Lin, S. H.; Lin, C.-K. *J. Chem. Phys.* **2011**, *135*, No. 104303.
(35) Kim, J. B.; Weichman, M. L.; Neumark, D. M. *Phys. Chem. Chem. Phys.* **2013**, *15*, 20973.
(36) Gong, Y.; Zhang, Q.; Zhou, M. *J. Phys. Chem. A* **2007**, *111*, 3534.
(37) Hagfeldt, A.; Bergstroem, R.; Siegbahn, H. O. G.; Lunell, S. *J. Phys. Chem.* **1993**, *97*, 12725.
(38) Albaret, T.; Finocchi, F.; Noguera, C. *J. Chem. Phys.* **2000**, *113*, 2238.
(39) Jeong, K. S.; Ch, C.; Sedlmayr, E.; Sülzle, D. *J. Phys. B: At., Mol. Opt. Phys.* **2000**, *33*, 3417.
(40) Qu, Z.-w.; Kroes, G.-J. *J. Phys. Chem. B* **2006**, *110*, 8998.
(41) Marom, N.; Kim, M.; Chelikowsky, J. R. *Phys. Rev. Lett.* **2012**, *108*, 106801.
(42) Hamad, S.; Catlow, C. R. A.; Woodley, S. M.; Lago, S.; Mejías, J. A. *J. Phys. Chem. B* **2005**, *109*, 15741.
(43) Ganguly Neogi, S.; Chaudhury, P. *J. Comput. Chem.* **2014**, *35*, 51.
(44) Chen, M.; Dixon, D. A. *J. Chem. Theory Comput.* **2013**, *9*, 3189.
(45) Li, S.; Dixon, D. A. *J. Phys. Chem. A* **2008**, *112*, 6646.
(46) Woodley, S. M.; Hamad, S.; Mejias, J. A.; Catlow, C. R. A. *J. Mater. Chem.* **2006**, *16*, 1927.
(47) Woodley, S. M.; Hamad, S.; Catlow, C. R. A. *Phys. Chem. Chem. Phys.* **2010**, *12*, 8454.
(48) Li, S. G.; Dixon, D. A. *J. Phys. Chem. A* **2010**, *114*, 2665.
(49) Osterwalder, A.; Nee, M. J.; Zhou, J.; Neumark, D. M. *J. Chem. Phys.* **2004**, *121*, 6317.
(50) Neumark, D. M. *J. Phys. Chem. A* **2008**, *112*, 13287.
(51) Hock, C.; Kim, J. B.; Weichman, M. L.; Yacovitch, T. I.; Neumark, D. M. *J. Chem. Phys.* **2012**, *137*, 224201.
(52) Eppink, A. T. J. B.; Parker, D. H. *Rev. Sci. Instrum.* **1997**, *68*, 3477.
(53) Kim, J. B.; Hock, C.; Yacovitch, T. I.; Neumark, D. M. *J. Phys. Chem. A* **2013**, *117*, 8126.
(54) Dick, B. *Phys. Chem. Chem. Phys.* **2014**, *16*, 570.
(55) Wigner, E. P. *Phys. Rev.* **1948**, *73*, 1002.
(56) Cooper, J.; Zare, R. N. *J. Chem. Phys.* **1968**, *48*, 942.
(57) Reid, K. L. *Annu. Rev. Phys. Chem.* **2003**, *54*, 397.
(58) Hay, P. J.; Wadt, W. R. *J. Chem. Phys.* **1985**, *82*, 299.
(59) Roy, L. E.; Hay, P. J.; Martin, R. L. *J. Chem. Theory Comput.* **2008**, *4*, 1029.
(60) Shao, Y.; Molnar, L. F.; Jung, Y.; Kussmann, J.; Ochsenfeld, C.; Brown, S. T.; Gilbert, A. T. B.; Slipchenko, L. V.; Levchenko, S. V.; O'Neill, D. P.; DiStasio, R. A., Jr.; Lochan, R. C.; Wang, T.; Beran, G. J. O.; Besley, N. A.; Herbert, J. M.; Yeh Lin, C.; Van Voorhis, T.; Hung Chien, S.; Sodt, A.; Steele, R. P.; Rassolov, V. A.; Maslen, P. E.; Korambath, P. P.; Adamson, R. D.; Austin, B.; Baker, J.; Byrd, E. F. C.; Dachsel, H.; Doerksen, R. J.; Dreuw, A.; Dunietz, B. D.; Dutoi, A. D.; Furlani, T. R.; Gwaltney, S. R.; Heyden, A.; Hirata, S.; Hsu, C.-P.; Kedziora, G.; Khalliulin, R. Z.; Klunzinger, P.; Lee, A. M.; Lee, M. S.; Liang, W.; Lotan, I.; Nair, N.; Peters, B.; Proynov, E. I.; Pieniazek, P. A.; Min Rhee, Y.; Ritchie, J.; Rosta, E.; David Sherrill, C.; Simmonett, A. C.; Subotnik, J. E.; Lee Woodcock, H., III; Zhang, W.; Bell, A. T.; Chakraborty, A. K.; Chipman, D. M.; Keil, F. J.; Warshel, A.; Hehre, W. J.; Schaefer, H. F., III; Kong, J.; Krylov, A. I.; Gill, P. M. W.; Head-Gordon, M. *Phys. Chem. Chem. Phys.* **2006**, *8*, 3172.
(61) Mozhayskiy, V. A.; Krylov, A. I. *ezSpectrum*, http://iopenshell.usc.edu/downloads.
(62) Cramer, C. J.; Truhlar, D. G. *Phys. Chem. Chem. Phys.* **2009**, *11*, 10757.
(63) Reed, K. J.; Zimmerman, A. H.; Andersen, H. C.; Brauman, J. I. *J. Chem. Phys.* **1976**, *64*, 1368.
(64) Taylor, D. J.; Paterson, M. J. *Chem. Phys.* **2012**, *408*, 1.